KFKI-1984-60

L. GRÁNÁSY
GY. MÉSZÁROS

MODELS FOR CONTINUOUS CASTING OF METALLIC GLASS RIBBONS

I: THE APPLICABILITY OF THE INFINITE VISCOSITY ASSUMPTION FOR THERMAL HISTORY CALCULATIONS

Hungarian Academy of Sciences

CENTRAL
RESEARCH
INSTITUTE FOR
PHYSICS

BUDAPEST

2017

KFKI-1984-60

MODELS FOR CONTINUOUS CASTING OF METALLIC GLASS RIBBONS

I: THE APPLICABILITY OF THE INFINITE VISCOSITY ASSUMPTION FOR THERMAL HISTORY CALCULATIONS

L. GRÁNÁSY, GY. MÉSZÁROS

Central Research Institute for Physics
H-1525 Budapest 114, P.O.B. 49, Hungary

HU ISSN 0368 5330
ISBN 963 372 246 2

ABSTRACT

In order to establish more reliable thermal history calculations we have examined how the melt flow influences the cooling process through convective heat transport. On the basis of the laminar boundary layer theory it has been shown that because of the continuous variation of viscosity around the glass transition the thermal history calculated with the assumption of infinite melt viscosity is very similar in a wide temperature region to that of computed with the experimental viscosity-temperature relation. It is illustrated for the $Fe_{40}Ni_{40}P_{14}B_6$ composition that this temperature region includes the range where TTT diagrams predict significant crystallization rates. On the other hand because of their mathematical simplicity, calculations with infinite viscosity allow to take into account those important experimental boundary conditions which cannot be properly treated in models including more detailed description of melt flow. In this way it is expected that calculations with infinite melt viscosity can reliably predict thermal history in the temperature region which is most important from the point of view of glass formation.

АННОТАЦИЯ

Для обоснования надежных расчетов термической предистории исследовалось влияние потока расплава на процесс охлаждения. На основании теории ламинарного граничного слоя было показано, что вследствие непрерывно увеличивающейся вязкости при стекловании, термическая предистория, при расчете которой предполагалась бесконечная вязкость, в широком температурном диапазоне показывает большую схожесть с результатами расчетов, выполненных на основе экспериментальной зависимости вязкости - температуры. На сплаве $Fe_{40}Ni_{40}P_{14}B_6$ иллюстрируется, что этот диапазон включает в себя и те температуры, при которых по диаграммам ТТТ важна скорость кристаллизации. С другой стороны простота математических расчетов, выполненных с бесконечной вязкостью, позволяет также учитывать и такие важные экспериментальные граничные условия, которые не могут быть учтены в модели, более подробно рассматривающей поток расплава. Таким образом можно ожидать, что расчеты, выполненные с бесконечной вязкостью, будут надежно описывать процесс охлаждения в важнейшем с точки зрения стеклования температурном диапазоне.

KIVONAT

A megbizható termikus elõélet-számitások megalapozásához megvizsgáltuk, hogyan befolyásolja az olvadékáramlás a hülés folyamatát. A lamináris határréteg elmélet alapján kimutattuk, hogy az üvegesedés során folytonosan növekvõ viszkozitás következtében a végtelen viszkozitás feltételezésével számitott termikus elõélet széles hõmérséklettartományban igen hasonló a kisérleti viszkozitás-hõmérséklet összefüggéssel számolthoz. A $Fe_{40}Ni_{40}P_{14}B_6$ ötvözet esetével illusztráltuk, hogy ez a tartomány magában foglalja azon hõmérsékleteket is, melyeknél a TTT diagramok szerint a kristályosodás sebessége lényeges. Másrészt a végtelen viszkozitással végzett számolások matematikai egyszerüsége miatt figyelembe vehetünk olyan fontos kisérleti határfeltételeket is, melyek nem kezelhetõek az olvadékáramlást részletesebben tárgyaló modellekben. Igy tehát azt várjuk, hogy a végtelen viszkozitással végzett számitások megbizhatóan irják le a hülés folyamatát az üvegképzõdés szempontjából legfontosabb hõmérséklettartományban.

1. INTRODUCTION

A relatively new group of amorphous materials is that of the metallic glasses. These materials - combining the disordered atomic arrangement with the metallic-type electronic structure - proved to be interesting from both theoretical and practical viewpoints. Metallic glasses are produced from the melt applying quenching rates high enough to avoid the crystallization during the solidification. Several methods have been developed to realize this purpose. Amorphous alloys are now available in quite different geometries (e.g. ribbon, surface layer, wire, powder, etc.) [1-4]. In the present paper we focuse our attention to the extensively investigated question how the metallic glass ribbon is formed in the continuous casting methods (i.e. in melt spinning, melt extraction and planar flow casting [5]). One of the most characteristic features of these methods is a melt pool produced in contact with a moving chill surface (substrate), as it is shown schematically in *Fig. 1.* The ribbon is formed from the (solidifying) melt layer dragged away by the substrate. According to the experiments glassy state is obtained below a given ribbon thickness (δ_{RC}) only. On one hand this critical ribbon thickness depends upon the critical quenching rate which may vary between wide limits due to the differences in the crystallization kinetics of the alloys [6,7]. On the other hand δ_{RC} is also influenced by the parameters which determine the efficiency of heat transport. It is the aim of several recent investigations to find the most important control parameters of metallic glass ribbon formation [8-16]. It is a priori clear that heat transport is determined - at least partially - by the heat diffusivity of the alloy, the substrate and by the heat transfer coefficient characteristic to the alloy-substrate interface. Naturally the role of the convective heat flow has also to be examined. It is a very complicated task because it requires the knowledge of the flow pattern inside the melt pool. The main difficulties arise from the fact that heat transport and melt flow interact through not only the convective heat flow but through the continuous temperature dependence of viscosity, characteristic to glass formation [17,18]. Several theoretical attempts have been published aimed at finding approximative flow patterns, but in the lack of direct experimental results* it is difficult to check the reliability of the thermal histories calculated in this way [12,14,15,20,24].

---

*Direct temperature distribution measurements are available for the melt spinning of crystalline alloys only, which - because of the evolution of latent heat - have limited relevance to amorphous ribbon formation [19].

The aim of the present paper is to find a mathematically simple approximation of melt flow, which - however - makes it possible to describe heat transport properly. In order to realize this program it is to be examined how the different supposed melt flow patterns influence heat transport. In this line first we classify the melt flow approximations, model calculations are then presented to illustrate the differences they cause in the heat transport. It is to be shown that as a consequence of the continuous variation of viscosity around the glass transition, the thermal history calculated with the assumption of infinite melt viscosity is very similar in a wide temperature region to that of computed with the experimental viscosity-temperature relation. It is also illustrated that this region includes the temperature range where the rate of crystallization is significant. In order to avoid the mathematical troubles these computations were performed under two somewhat unrealistic suppositions referring to heat transport. It is however suggested that the above similarity of thermal histories remains valid also under realistic conditions. On the other hand the calculations with infinite viscosity are relatively simple, i.e. all the important thermal boundary conditions can be taken into account. It is thus suggested that the infinite viscosity approximation is an appropriate tool for the determination of thermal history.

2. FLOW PATTERN APPROXIMATIONS

In this point we briefly survey the most important flow pattern approximations. The following main processes have to be taken into account in a detailed thermal history calculation:

a) Heat flow in the melt pool (including both the conductive and the convective modes of heat transport, the effect of the temperature dependence of viscosity and the complicated boundary conditions),
b) Heat flow in the solidified region,
c) Heat transfer at the alloy-substrate interface,
d) Heat flow within the substrate.

These processes are closely cross-connected through the conservation of energy, making the full realization of such a calculation unjustified in terms of computation cost. Simplifications are needed. Since the most difficult problem is that of modelling the melt flow, a supposed simple flow pattern may significantly reduce the complexity of the mathematical task. On the other hand one may only hope that this modification does not significantly disturb the calculated thermal history. This hope motivates the use of the flow pattern approximations in thermal history calculations. There is however another aspect of melt flow modelling: A detailed description of the melt pool may facilitate the testing of the basic assumptions. Since simplifications referring to either the melt flow or the heat transport may be

reflected in the melt pool length-ribbon thickness relation [8,14,15,25,26], the comparison of the calculated and experimental relations may inform us about the validity of the applied approximations.

2.1 Infinite viscosity approximations

Up to now the majority of the thermal history calculations [14,15,20,22] is based on an approximation, which describes the heat transport by the one-dimensional heat diffusion equation*:

$$\frac{\partial T}{\partial t} = \chi \frac{\partial^2 T}{\partial y^2} \qquad (1)$$

(The meaning of all the symbols is listed in Notations.) We have to emphasize, however, that this approximation means special restrictions referring to the melt flow: It is easy to show that the application of the transformation, $x=V_o t$ yields a two-dimensional, steady state problem, which can also be obtained from the boundary layer theory (BLT) of heat transport in fluids [28] assuming infinite viscosity. Consequently this generally used approximation is physically equivalent to the supposition of infinite melt viscosity. This kind of simplification has a great advantage: The melt region and the solid phase may be treated uniformly, which significantly reduces the mathematical troubles. On the other hand, because of the neglection of the details of the melt flow, the length of the melt pool cannot be calculated within the frame of this approximation.

2.2 Constant viscosity approximations

Several attempts have been made recently to describe the melt flow more precisely. In most of them melt is characterized by a fixed (and finite) value of viscosity. Under such conditions the most detailed description of melt flow and heat transport is given by the BLT. Because of the mathematical difficulties, however, boundary layer calculations of this field are generally restricted to the modelling of melt flow only [14,15,30], while in the determination of the thermal history special heat transport conditions [31] or simplified boundary layer equations [23,24] are used.

---

*The widely used Newtonian-type cooling is also a special case of this approximation when $h \ll \frac{\kappa}{\delta_R}$ (see e.g. [27]).

2.3 Temperature dependent viscosity approximations

Since the drastical increase of melt viscosity during the glass formation may significantly influence the melt flow and convective heat transport, efforts have been done to take this effect also into account [31]. Such a detailed characterization of the melt is only meaningful, however, within the frame of BLT. On the other hand the application of BLT leads to restrictions of technical origin: In order to avoid the mathematical complexity, special heat transport conditions have to be supposed. Hence the advantage of the detailed description of melt flow is countered by the inadequate description of heat transport. In spite of this fact this model provides a unique facility to compare the melt flow approximations under given though somewhat non-realistic conditions.

3. MODEL CALCULATIONS

Let us first give a short summary of the model our study is based on and examine its applicability to the description of the ribbon formation process. Second, in order to illustrate the physical consequences of the different melt flow approximations we present the results obtained using the viscosity-temperature relations distincted in the previous point. Finally we discuss the origin of the differences and outline the application of the infinite viscosity approximation for realistic thermal history calculations.

3.1 The model

In our calculations we started from a construction which is similar to that of den Decker and Drevers [31]. The main difference is that heat transport within the substrate is also taken into account. The basic features of the original model are the following:

- two-dimensional system,
- steady-state solution,
- ideal heat contact at the alloy-substrate interface,
- temperature independent properties (except viscosity),
- laminar BLT for the description of melt flow*,
- the melt and the solidified phase fill in the whole $x,y>o$ quarter-plane.

---

*The laminarity of melt flow is a questionable assumption, since experimental results pro and contra are also available [14,32]. On theoretical basis, however, it is expected that because of the high value of viscosity in the vicinity of T_g there has to be an extended laminar sublayer preceding the solidification front.

We contributed to the list with a simplification which refers to the substrate:

- the substrate fills in the whole x>o, y<o quarter-plane.

Since our basic equations are derived in a way which is general in the practice of BLT we simply present them and refer to sources where the mathematical procedure is detailed [28,29,31]:

Equations:

Melt phase: $$\nu f''' + \nu' f'' + \chi_L f'' f = 0 \qquad (2.a)$$

$$\tau''_L + f\tau'_L = 0 \qquad (2.b)$$

$$\nu = \nu(\xi_L) \qquad (2.c)$$

Solid phase: $$\tau''_S + 2\xi_S \tau'_S = 0 \qquad (2.d)$$

Substrate: $$\tau''_{Su} + 2\xi_{Su}\tau'_{Su} = 0 \qquad (2.e)$$

where subscripts L,S,Su refer to the melt, the solid and the substrate, respectively; $\tau_{L,S,Su} = 2\,\frac{T_{L,S,Su}-T_o}{T_M-T_o}$ and $\xi_{L,S,Su} = \frac{y}{2}\left(\frac{V_o}{x\,\chi_{L,S,Su}}\right)^{1/2}$ are the reduced temperature and the parabolic coordinate of the corresponding phase, f is a function related to the velocity distribution as follows:

$$v_x(x,y) = \frac{V_o}{2} f'(\xi_L) \qquad (3)$$

$$v_y(x,y) = \frac{1}{2}\left(\frac{V_o \chi_L}{x}\right)^{1/2} \{f'(\xi_L)\xi_L - f(\xi_L)\}, \qquad (4)$$

while f',τ',ν' etc. are functions differentiated with respect to the parabolic coordinates.

The boundary conditions corresponding to the basic assumptions are:

$$f(\xi_{Lo}) = 2\xi_{Lo} \quad f'(\xi_{Lo}) = 2 \quad f'(\infty) = 0 \qquad (5.a,b,c)$$

$$\tau_L(\xi_{Lo}) = \tau_g \quad \tau_L(\infty) = 2 \qquad (5.d,e)$$

$$\frac{\kappa_L}{\sqrt{\chi_L}}\tau'_L(\xi_{Lo}) = \frac{\kappa_S}{\sqrt{\chi_S}}\tau'_S(\xi_{So}) \qquad (5.f)$$

$$\tau_S(\xi_{So}) = \tau_g \quad \tau_S(o) = \tau_{Su}(o) \quad \tau_{Su}(-\infty) = 0 \qquad (5.g,h,i)$$

$$\frac{\kappa_S}{\sqrt{\chi_S}}\tau'_S(o) = \frac{\kappa_{Su}}{\sqrt{\chi_{Su}}}\tau'_{Su}(o) \qquad (5.j)$$

where ξ_{Lo}, ξ_{So} are the position of the solidification front expressed in terms of the parabolic coordinates, while $\tau_g = 2\frac{T_g - T_o}{T_M - T_o}$. In this calculation the position of the solidification front is initially unknown. It is determined as follows: Starting from an approximate value of ξ_{Lo} the mathematical problem of the melt phase may be separated from that of the remaining part, consequently the two sets of equations obtained in this way can be solved independently. The right position of the solidification front may be found iteratively on the basis of (5.f).

In our work the solid phase and the substrate were treated analitically (see Appendix 1), while numerical solutions based on the finite difference method were derived for the melt phase. In principle the numerical treatment of the melt region allows the solution of the problem for any type of viscosity functions. The analytical treatment, however, has several advantages, that is why we developed analytical solutions for the simplest (zero and infinite viscosity) cases (see Appendix 2).

Having determined the temperature and velocity distributions we are able to calculate either the relation between the melt pool length and the ribbon thickness or the thermal history. The relation between melt pool length and ribbon thickness may be derived following the way proposed by den Decker and Drevers. The method is visualized in *Fig. 2*. Stream lines are given by the $\Phi(x,y) = \text{const.}$ relations, where $\Phi(x,y) = (V_o \chi_L x)^{1/2} f(\xi_L)$ is the stream function [28,29]. Starting from (5.a-c) it can be shown that stream lines are parallel to the y-axis for $y \to \infty$. On the other hand they are naturally parallel to the x-axis in the solid region. Being aware of these facts melt pool length corresponding to a given ribbon thickness may be constructed as follows: Let us find the stream line which intersects the solidification front at height $y = \delta_R$, then remove the region above it (see Region 2 in Fig. 2). The remaining part represents the melt pool-ribbon-substrate system. The length of the melt pool may be defined by the distance between the y-axis and this stream line when $y \to \infty$. Taking into account this definition, the volumetric flow balance, expression (4) and the fact that $\lim_{\xi_L \to \infty} f'(\xi_L)\xi_L = 0$ it is easy to show that

$$\delta_R = f(\infty) \left(\frac{\chi_L \ell}{V_o}\right)^{1/2} \tag{6}$$

where $f(\infty) = \lim_{\xi_L \to o} f(\delta_L)$ is a proportionality factor, which depends on T_M, $T_o, \nu(T), \chi_L, \chi_S, \chi_{Su}$.

Thermal history along stream lines can also be determined from the calculated temperature and velocity distributions. It can be shown that as a straightforward consequence of the supposed ideal heat contact and laminar melt flow the average quenching rate, $\bar{\dot{T}} = \left|\frac{T_m - T_S}{t_{T_m} - t_{T_g}}\right|$ is proportional to δ_R^{-2}

(see Appendix 3). The quenching rate values derived in this way are, however, to be accepted as a rough approximation only: The removal of Region 2 significantly changes the upper boundary condition of heat transport in Region 3, i.e. the substrate has to extract heat from a layer of finite thickness instead of the original infinite region. Consequently a significant increase of cooling rate is expected. Naturally this acceleration of cooling has to be manifested in melt pool shortening too, but it is not clear in what extent. The modifications required by this "thickness effect" cannot be easily incorporated to the present model.

Supposition of ideal heat contact at the alloy-substrate interface seems to be another serious shortcoming of the construction. Experimental results suggest that ideal heat contact may be an approximation of questionable validity [12,19]. The existence of an interfacial heat resistance between the substrate and the alloy may significantly reduce heat extraction [27,33], its treatment is however complicated within the realistic fluid flow model.

3.2 Testing of the model

Summarizing the problematic features of the model we have to emphasize that two unjustified simplifications are built in, which have opposite effect on either the melt pool length or the quenching rate. In order to check the applicability of these assumptions we compare the calculated melt pool length-ribbon thickness relation to its experimental counterpart. Alloys with composition $Fe_{40}Ni_{40}P_{14}B_6$ and $Fe_{80}P_{13}C_7$ have been chosen as testing materials, while a copper substrate has been supposed. The relevant physical properties are given in Appendix 4.

A typical melt pool structure calculated for $Fe_{40}Ni_{40}P_{14}B_6$ under V_o = 30 m/s and δ_R = 30 μm is shown in *Fig. 3*. Because of the steady state solution the path of volume elements is given by the stream lines. In this way, first the volume elements move parallel to the y-axis and then penetrate into the shear layer (or momentum boundary layer, defined by $0.05\ V_o<v_x<V_o$), where the x component of their velocity increases up to V_o, while v_y tends to zero. Intersecting the solidification front the paths enter the solid region. It is worth mentioning that as a consequence of the continuous increase of melt viscosity the solidification front is preceded by an extended quasi-solid layer defined by the $0.95\ V_o<v_x<V_o$ relation.

The results of melt pool length calculations are summarized in Tables 1, 2. It shows that the calculated melt pools are significantly shorter then their experimental counterparts for both compositions studied. The sensitivity analysis of the solutions has shown that this deviation cannot be understood on the basis of either the experimental error of the relevant physical properties or the temperature dependence of those parameters which were fixed

in the calculations (c_p, κ, ρ, T_g). Thus the origin of the deviations must be one of the assumptions the model is based on. Since viscosity is a monotonously decreasing function of temperature, the underestimation of melt pool length must be the result of an overestimated heat extraction, i.e. the supposition of ideal heat contact seems to be responsible for the deviations.

3.3 The effect of melt flow approximations on the thermal history

In this point we intend to show what kind of differences arise between thermal histories calculated using different types of viscosity-temperature relations distincted in 2. In order to realize this comparative analysis computations were performed with viscosity functions $\nu = o$, $\nu = \nu_F(T_M)$, $\nu = \nu_F(T)$ and $\nu = \infty$, where the F subscripts refer to the Fulcher-type temperature dependence of viscosity, $\nu_F(T) = \nu_o \exp\{\frac{W}{T-T_F}\}$ characteristic to supercooled melts. In these simulations $\nu_F(T_M)$, $\nu_F(T)$ and the other relevant parameters were chosen to be identical to those of the $Fe_{40}Ni_{40}P_{14}B_6$ alloy. Thus we obtained a series in which the average value of viscosity, $\bar{\nu}$ is changed systematically.

Melt pool structures calculated under such conditions are shown in *Fig. 4*, while some characteristic parameters are given in Table 3. As it could be expected on the basis of BLT, the thickness of the momentum boundary layer is sensitive to the viscosity-temperature relation. As a consequence the length of the melt pool is decreasing, while $f(\infty)$ is increasing with increasing $\bar{\nu}$. At the same time a remarkable variation of the temperature distribution is indicated by the position of the T_m and T_g isotherms. The solidification length, ℓ_o - i.e. the x coordinate where the temperature of the ribbon drops below T_g even at the top surface - is also changed. Summarizing these tendencies we may conclude that the variation of the viscosity function influences the structure of the melt pool through two opposing effects:

a) Mechanical effect: In accordance with the predictions of BLT, the higher is the value of the average viscosity, the thicker is the momentum boundary layer, consequently the shorter is the melt pool.
b) Thermal effect: The higher is $\bar{\nu}$, the higher is the average value of v_x, i.e. a more effective convection occures between the T_M and T_g isotherms. As a straightforward consequence the solidification front is lowered, i.e. the solidification length increases. Because of this lowering of the base of the boundary layer the length of the melt pool is also increased.

The average quenching rates calculated along stream lines corresponding to $\delta_R = 30$ μm are also given in Table 3. Despite the monotonous variation of the solidification length, $\bar{\dot{T}}$ shows a maximum, suggesting that ℓ_o cannot be accepted as a parameter characteristic to thermal history when materials

of significantly different viscosity functions are compared. The reason is obvious: Thermal history depends on not only the temperature distribution but also on the velocity field (i.e. on the shape of the stream line and on the distribution of the tangential velocity along it), while ℓ_o is determined by merely the position of the T_g front. Another interesting fact is the similarity of the T values calculated for $\nu = \infty$ and $\nu = \nu_F(T)$ which indicates the similarity of the corresponding cooling processes. T(t) curves describing the details of thermal history between T_m and T_g are presented in *Fig. 5*. The most remarkable consequence of these plots is that viscosity functions $\nu = \infty$ and $\nu = \nu_F(T)$ provide of almost identical cooling conditions in the whole $T_m > T > T_g$ temperature region. It has to be emphasized, however, that this similarity is soon deteriorated for $T > T_m$. It is easy to understand this behaviour on the basis of Fig. 4. From the position of the T_M, T_m and T_g isotherms it is clear that temperature distributions are roughly similar in the $\nu = \infty$ and $\nu = \nu_F(T)$ bases. On the other hand because of the presence of the quasi-solid layer the shape of the stream lines is almost identical between T_m and T_g, while significant differences can be seen at higher temperatures. These differences are manifested in the time measured between the T_M and T_m isotherms moving along stream lines: $\Delta t = \infty$ for $\nu = \nu_F(T)$ and $\Delta t < \infty$ for $\nu = \infty$. Thus above T_m quenching rate becomes much lower for $\nu = \nu_F(T)$ than for $\nu = \infty$. This tendency is directly visualized in *Fig. 6*, where the momentary quenching rate is plotted versus the actual temperature. In this way we may conclude that as a consequence of the special viscosity-temperature relation of the supercooled glass forming alloys there appeares an extended "quasi-solid" layer above the solidification front, which provides of cooling conditions similar to those of the $\nu = \infty$ case in a wide temperature region.

This similarity may have an important role in thermal history calculations: From the point of view of glass formation thermal history is interesting in a limited temperature region only, where the rate of crystallization is high enough to be taken into account on the time scale of the quenching process. Consequently calculations which correctly describe cooling in this region would be of practical importance. In the case of the $Fe_{40}Ni_{40}P_{14}B_6$ composition TTT diagrams predict significant transformation rates between 800 and 1000 K [34,35], which region is within the range where $\nu = \nu_F(T)$ and $\nu = \infty$ give similar thermal history. In this way our calculations justified the use of the $\nu = \infty$ approximation when simplifications listed in 3.1 are valid. On the other hand it requires further discussions to understand what kind of differences can be expected when the non-ideal heat contact and the sudden change of boundary conditions at $x = \ell$ are taken into account.

If the heat contact at the alloy-substrate interface is non-ideal (i.e. the heat transfer coefficient is finite, $h < \infty$) heat extraction from the alloy is hindered. It is easy to show that $\ell_o \to \infty$ and $T_L(x,y) \to T_M$ if $h \to o$. Thus when $h = o$ there is no solidification and the melt can be characterized by a fixed viscosity value, $\nu = \nu_F(T_M)$. Under such conditions the length of the melt pool is finite, determined by the

$$\ell^* = \frac{V_o}{\nu_F(T_M)} \left(\frac{\delta_R}{1.62}\right)^2 \qquad (7)$$

formula derived in Appendix 5. Consequently $\ell/\ell_o \to o$ when $h \to o$ indicating that the region where the stream lines of the $\nu = \infty$ and $\nu = \nu_F(T)$ cases are of different shape becomes negligible. In other words: The penetration depth of the thermal effect becomes far less than that of the momentum transport, consequently $v_x \cong V_o$ in the whole region where heat transport takes place. In this way we may expect that decreasing the value of h the similarity of cooling processes corresponding to $\nu = \infty$ and $\nu = \nu_F(T)$ is more and more pronounced.

The other modification the presented model has to be completed with is the "thickness effect". Its influence on the examined similarity of thermal histories cannot be predicted so easily as in the former case. On logical ground, however arguments are found which support the applicability of the $\nu = \infty$ approximation also under this condition:

Let us discuss the problem in the hypothetical case of ideal heat contact. When Region 2 (see Fig. 2) is removed a new thermal boundary condition has to be prescribed along the stream line corresponding to δ_R. Since the effect of heat radiation can be neglected, $\frac{\partial T}{\partial n} = o$ seems to be an adequate assumption, where n stands for the normal of the boundary stream line. This change in the boundary conditions may significantly influence heat transport in the $x \gtrsim \ell$ region and may also modify the length of the melt pool. For $x > \ell$ henceforth heat is extracted from a thin layer the heat content of which can fastly be exhausted, leading to a significant increase of the quenching rate. We have to emphasize, however, that the new boundary condition is automatically satisfied outside the thermal boundary layer, where $T_L(x,y) \cong T_M$. In this way modifications of the temperature distribution are expected within the thermal boundary layer only. On the other hand the penetration depth of the thermal effects (δ_T) is small compared to the length of the melt pool (it is easy to show that in the case of laminar flow and ideal heat contact $\frac{\delta_T}{\ell} \sim Pè^{-1/2}$, where $Pè = \frac{V_o \ell}{\chi_L}$ is the Pèclet number, in our case $Pè \gtrsim 10^4$, resulting in that $\delta_T \ll \ell$), which indicates that within the momentum boundary layer the thermal conduction in direction x is overrun by the thermal convection. This fact implies that the effect of the new boundary condition at $x = \ell$ cannot penetrate deep into the melt pool. The presented model is thus expected to be able to predict the temperature distribution within the melt pool, when ideal heat contact is supposed. As in the case of $\nu = \infty$ and $\nu = \nu_F(T)$ viscosity functions our calculations predict similar temperature distributions even in those regions where the velocity fields are significantly different it is somewhat justified to expect that the same variation of the thermal boundary conditions will modify temperature distributions analogously for $x \gtrsim \ell$, where the velocity distributions are necessarily more similar.

Summarizing the consequences of the above argumentation we may expect that $\nu = \infty$ calculations which take into account the "thickness effect" and non-ideal heat contact may be regarded as reliable models of thermal history in the region of significant crystallization rates. Calculations of this type will be presented in the near future [36].

4. SUMMARY

The influence of melt flow on heat transport and thermal history has been studied within the frame of boundary layer theory. It has been shown that:

1. Since the complexity of the model does not make it possible to incorporate the "thickness effect" and the non-ideal heat contact between the alloy and the substrate, the full treatment of melt flow proposed by den Decker and Drevers cannot correctly predict either the length of the melt pool or the thermal history.

2. Because of the special viscosity-temperature relation of glass forming alloys, there exists an extended temperature region where calculations with the $\nu = \infty$ assumption and with the experimental viscosity function give very similar cooling processes. This temperature region contains also the range where TTT diagrams prescribe the highest crystallization rates.

3. On theoretical ground $\nu = \infty$ calculations completed with non-ideal heat transfer and "thickness effect" are expected to be able to reliably predict thermal history.

ACKNOWLEDGEMENT

We are very grateful to Dr. T. Kemény for the valuable discussions and the critical reading of the manuscript.

REFERENCES

[1] H. Jones, Rapid Solidification Processing, ed. R. Mehrabian (Claitor's Publishing Division, 1978) p. 28 and
H. Jones, in "Treatise on Materials Science and Technology", Vol. 20, ed. H. Herman (Academic Press, New York, 1981) p. 1

[2] H.S. Chen, H.J. Leamy, C.E. Miller, Ann. Rev. Mater. Sci., 10/1980/363

[3] Rapidly Quenched Metals IV., eds. T. Masumoto and K. Suzuki (The Japan Institute of Metals, 1982)

[4] Proc. Symp. on Continuous Casting of Small Cross Sections, eds. Y.V. Murty and F.R. Mollard (AIME, Warrendale, Pa, 1981)

[5] Melt spinning, e.g.: H.H. Liebermann, C.D. Graham, IEEE, Trans. on Magn., 12/1976/921,
melt extraction, e.g.: R.E. Maringer, C.E. Mobley and E.W. Collins, Rapidly Quenched Metals, eds. N.J. Grant and B.C. Giessen (MIT Press, Boston, 1975) p. 29,
planar flow casting, e.g.: M.C. Narasimhan, US Patent No 3862658 (1975)

[6] M. Hagivara, A. Inoue, T. Masumoto, Sci. Rep. RITU A29/1981/351

[7] H.A. Davies, Rapidly Quenched Metals III., ed. B. Cantor, (The Metals Society, 1978) Vol. 1, p. 1

[8] H. Hillmann, H.R. Hilzinger, ibid., Vol. 1, p. 22

[9] H.H. Liebermann, Mater. Sci. Eng., 43/1980/203

[10] S. Takayama, T. Oi, J. Appl. Phys., 50/1979/4962

[11] S.C. Huang, H.C. Fiedler, in [4], p. 127

[12] S.C. Huang, H.C. Fiedler, Mater. Sci. Eng., 51/1981/39

[13] D. Pavuna, J. Mater. Sci., 16/1981/2419

[14] J.H. Vincent, H.A. Davies, J.G. Herbertson, in [4], p. 103

[15] J.H. Vincent, J.G. Herbertson, H.A. Davies, in [3], Vol. 1, p. 77

[16] M. Matsuura, M. Kikuchi, M. Yagi, K. Suzuki, Japn. J. Appl. Phys., 19/1980/1781

[17] H. Vogel, Phys. Z., 22/1921/645

[18] G.S. Fulcher, J. Ann. Ceram. Soc., 6/1925/339

[19] D.H. Warrington, H.A. Davies, N. Shohoji, in [3], Vol. 1, p. 69

[20] L. Katgerman, Script. Metall., 14/1980/861

[21] L. Katgerman, P.J. van den Brink, in [3], Vol. 1, p. 61

[22] S. Kavesh, "Metallic Glasses", eds. J.J. Gilman and H.J. Leamy, (ASM, 1976) p. 36

[23] T.R. Anthony, H.E. Cline, J. Appl. Phys., 49/1978/829

[24] T.R. Anthony, H.E. Cline, J. Appl. Phys., 50/1979/239

[25] J.H. Vincent, J.G. Herbertson, H.A. Davies, J. Mater, Sci. Letters, 2/1983/88

[26] L. Gránásy, T. Kemény, Central Research Institute for Physics Report, KFKI-1982-32

[27] R.C. Ruhl, Mater, Sci. Eng., 1/1967/313

[28] L.D. Landau, E.M. Lifshitz, "Fluid Mechanics", Pergamon Press, New York (1959)

[29] H. Schlichting, "Boundary Layer Theory", 6th Edition, McGraw Hill (1966)

[30] P.H. Shingu, K. Kobayashi, R. Suzuki, K. Takeshita, in [3], Vol. 1, p. 57

[31] P. den Decker, A. Drevers, Proc. Conf. on Metallic Glasses: Science and Technology (Kultura, 1981) Vol. 1. p. 181

[32] P.G. Zielinski, D.G. Ast, Script. Metall., 17/1983/291

[33] P.H. Shingu, R. Ozaki, Metall. Trans., 6A/1975/33

[34] P.M. Anderson, A.E. Lord, J. Non-Cryst. Solids, 37/1980/219

[35] D.G. Morris, Acta Metall., 29/1981/1213

[36] L. Gránásy and Gy. Mészáros, under preparation

[37] M.G. Scott, P. Ramachandrarao, Mater. Sci. Eng., 29/1977/137

[38] J.A. Adams, D.F. Rogers, "Computer Aided Heat Transfer Analysis", McGraw Hill (1963)

NOTATIONS

T - temperature
T_M - initial temperature of the melt
T_m - melting temperature
T_g - temperature of the glass transition
T_F - temperature parameter of the Fulcher-formula
T_o - initial temperature of the substrate
τ - reduced temperature
t - time
Δt - time period measured between the T_M and T_m isotherms along stream lines
$t_{T_m} - t_{T_g}$ - time period measured between the T_m and T_g isotherms along stream lines
$\dot{T}$ - quenching rate
$\overline{\dot{T}}$ - average quenching rate
h - heat transfer coefficient at the alloy-substrate interface
χ - heat diffusivity defined by $\chi = \frac{\kappa}{\rho C_p}$, where
κ - heat conductivity
ρ - density
c_p - specific heat
x - coordinate parallel to the surface of the substrate measured in the direction of moving
y - coordinate perpendicular to the surface of the substrate
ξ - parabolic coordinate
ξ_o - position of the solidification front
ℓ - melt pool length
ℓ^* - limiting value of melt pool length corresponding to $h \to o$
ℓ_o - solidification length
δ_R - ribbon thickness
δ_{RC} - critical ribbon thickness
δ_T - penetration depth of thermal effect
v_x, v_y - components of the velocity vector
V_o - surface velocity of the substrate
Φ - stream function
ν - kinematic viscosity
$\overline{\nu}$ - average viscosity
$\operatorname{erf} x$ - $\frac{2}{\sqrt{\pi}} \int_o^x e^{-t^2} dt$
Pè - Pèclet number

Subscripts L,S,Su refer to the melt, the solid phase and the substrate respectively.

Table 1

Comparison of the calculated melt pool length-ribbon thickness relation with experiments [8] in case of $Fe_{40}Ni_{40}P_{14}B_6$

V_o (m/s)	δ_R (μm)	ℓ_{exp} (mm)	ℓ_{calc} (mm)
15	55	5.3	2.26
30	31	3.7	1.44
60	18	2.7	0.97

Table 2

Comparison of the calculated and experimental [14] melt pool length-ribbon thickness relations in case of $Fe_{80}P_{13}C_7$

V_o (m/s)	δ_R (μm)	ℓ_{exp} (mm)	ℓ_{calc} (mm)
20	37	3.5	0.72
30	26	3.1	0.57
40	20	3.0	0.42

Table 3

The effect of viscosity function on the parameters characteristic to the melt pool structure and thermal history

$\nu(T)$	ℓ (mm)	$f(\infty)$	ℓ_o (mm)	$\dot{\bar{T}}$ (10^6 K/s)
$\nu = 0$	5.81	0.94	5.81	0.36
$\nu = \nu_F(T_M)$	4.43	1.08	6.78	0.58
$\nu = \nu_F(T)$	1.34	1.95	13.6	1.00
$\nu = \infty$	0	∞	16.3	0.85

$\dot{\bar{T}}$, ℓ, ℓ_o values corresponding to δ_R = 30 μm and V_o = 30 m/s are presented.

APPENDIX 1

Analytical treatment of heat transport in the solid phase and the substrate

Solutions of the form

$$\tau_S(\xi_S) = A_S + B_S \text{ erf } (\xi_S) \qquad \text{and} \qquad \text{(A1)}$$

$$\tau_{Su}(\xi_{Su}) = A_{Su} + B_{Su} \text{ erf } (\xi_{Su}) \qquad \text{(A2)}$$

were fitted to boundary conditions (5g-j). The temperature distributions obtained in this way are

$$\tau_S(\xi_S) = \frac{\tau_q(1+B \text{ erf } (\xi_S))}{1 + B \text{ erf } (\xi_{So})} \qquad \text{and} \qquad \text{(A3)}$$

$$\tau_{Su}(\xi_{Su}) = \frac{\tau_q(1 + \text{erf } (\xi_{Su}))}{1 + B \text{ erf } (\xi_{So})} \qquad \text{(A4)}$$

where $B = \frac{\kappa_{Su}}{\kappa_S}\sqrt{\frac{\chi_S}{\chi_{Su}}}$.

APPENDIX 2

Analytical treatment of the melt phase in cases of infinite and zero viscosity

It is easy to show that in the $\nu \to \infty$ limit $v_x = V_o$ within the whole x,y>o region (i.e. the thickness of the momentum boundary layer is infinite). In accordance with this fact:

$$\left.\begin{aligned} f'(\xi_L) &= 2\Theta(\xi_L - \xi_{Lo}) \\ f(\xi_L) &= 2\xi_L \end{aligned}\right\} \quad \text{and} \quad \text{for } \xi_L > \xi_{Lo} \qquad \text{(A5a,b)}$$

where $\Theta(x)$ is the Heavyside-function. Inserting (A5b) into (2b) heat transport equation of the form

$$\tau''_L + 2\xi_L \tau'_L = 0 \qquad \text{(A6)}$$

is obtained. Its solution which satisfies boundary conditions (5d,e) is the following:

$$\tau_L(\xi_L) = \frac{\tau_g - 2\ \mathrm{erf}\ (\xi_{Lo}) + (2-\tau_g)\ \mathrm{erf}\ (\xi_L)}{1 - \mathrm{erf}\ (\xi_{Lo})} \ . \qquad \text{(A7)}$$

The assumption $\nu = o$ results in zero thickness of the momentum boundary layer which means that $v_x = o$ above the solidification front. Its mathematical formulation is:

$$\left.\begin{aligned} f'(\xi_L) &= 2[1-\Theta(\xi_L-\xi_{Lo})] \\ f(\xi_L) &= 2\xi_{Lo} \end{aligned}\right\} \quad \text{and} \quad \text{for} \quad \xi_L > \xi_{Lo} \qquad \text{(A8a,b)}$$

leading to

$$\tau''_L + 2\xi_{Lo}\tau'_L = o \ . \qquad \text{(A9)}$$

The solution found by the integration of (A9) was fitted to (5d,e) yielding

$$\tau_L(\xi_L) = 2-(2-\tau_g)\ \exp\ [-2\xi_{Lo}(\xi_L-\xi_{Lo})] \ . \qquad \text{(A10)}$$

APPENDIX 3

Determination of the relation between the average quenching rate and the thickness of the ribbon

Since the stream line corresponding to δ_R is given by the implicite equation

$$\Phi_{\delta_R} = V_o\delta_R = (V_o\chi_L x)^{1/2} f(\xi_L) \qquad \text{(A11)}$$

it is easy to show that the x coordinate of the points where the T_m and T_g isotherms intersect the stream line are of the form $x_m = c_m\delta_R^2$ and $x_g = c_g\delta_R^2$ denoting $V_o\chi_L^{-1}[f(\xi)]^{-2}$ with c. On the other hand

$$\bar{\dot{T}} = \left|\frac{T_m - T_g}{t_{T_m} - t_{T_g}}\right| = \left|\frac{(T_m - T_g)\bar{v}}{x_m - x_g}\right| \qquad \text{(A12)}$$

and

$$\bar{v} = \frac{1}{x_g - x_m}\int_{x_m}^{x_g} v_x(x,y)\,dx = \frac{V_o}{2(x_g - x_m)}\int_{x_m}^{x_g} f'\{\xi(x)\}dx \qquad \text{(A13)}$$

where the integration with respect to x has to be performed along the stream line. On the basis of (A11) ξ can be expressed in terms of x:

$$\xi(x) = f^{-1}\left(\delta_R \sqrt{\frac{V_o}{\chi_L x}}\right) \tag{A14}$$

where f^{-1} is the inverse function of f. Inserting (A14) into (A13) and introducing $\zeta = x\delta_R^{-2}$ as a new variable

$$\bar{v} = \frac{V_o}{2(c_g - c_m)} \int_{c_m}^{c_g} f'\left(f^{-1}\sqrt{\frac{V_o}{\chi_L \zeta}}\right)\Big\} d\zeta \tag{A15}$$

is obtained, indicating that $\bar{v}$ is independent of δ_R. In this way

$$\bar{\dot{T}} = \left|\frac{(T_m - T_g)\bar{v}}{(c_m - c_g)\delta_R^2}\right| \sim \frac{1}{\delta_R^2} .$$

APPENDIX 4

Casting conditions and the physical properties of the alloys and the substrate used in modelling

a) Casting conditions

T_o = 293 K, while T_M = 1323 K for $Fe_{40}Ni_{40}P_{14}B_6$ and T_M = 1300 K for $Fe_{80}P_{13}C_7$. Having determined the numerical value of $f(\infty)$ the V_o dependence of melt pool length can be treated analytically according to (6), while $\dot{T}$ is independent of V_o when δ_R is fixed.

b) Physical properties

Heat conductivity, specific heat and density were taken to be identical for the two alloys and for the solid and melt phases:

$\kappa_L = \kappa_S$ = 21 W/mK, $c_{pL} = c_{pS}$ = 540 J/kgK, $\rho_L = \rho_S$ = 7400 kg/m^3.

The differences of the viscosity function, melting point and T_g were taken into account:

$Fe_{40}Ni_{40}P_{14}B_6$ parameters taken from [34,35]:

$$\nu(T) = 6.6\times10^{-9} \exp\left(\frac{3312.6}{T-575}\right) \frac{m^2}{s} ,$$

T_m = 1173 K, T_g = 750 K,

where the value of T_g is a result of an extrapolation for high quenching rates (10^7 K/s).

$Fe_{80}P_{13}C_7$ parameters taken from [7,37]:

$$\nu(T) = 3\times10^{-9} \exp\left(\frac{4600}{T-616}\right) \frac{m^2}{s}$$

$$T_m = 1260 \text{ K}, \quad T_g = 850 \text{ K},$$

where T_g is estimated from the heating rate dependence of the crystallization temperature.

In all the calculations a copper substrate characterized by the following properties was used:

$$\kappa_{Su} = 380 \text{ W/mK}, \quad c_{pSu} = 420 \text{ J/kgK}, \quad \rho_{Su} = 8900 \text{ kg/m}^3 .$$

APPENDIX 5

Derivation of Eq. (7)

When constant viscosity is supposed the velocity field in the momentum boundary layer is described by the special form of the Faulkner-Skan equation [38] known as Blasius equation:

$$f''' + ff'' = 0 \tag{A16}$$

where f relates to the velocity distribution according to formulae (3,4) after replacing χ_L by ν. The boundary conditions corresponding to our problem are:

$$f(0) = 0 \qquad f'(0) = 2 \qquad f'(\infty) = 0 \tag{A17}$$

The relation between the melt pool length and the ribbon thickness can be derived analogously to (6):

$$\delta_R = f(\infty) \left(\frac{\nu \ell}{V_o}\right)^{1/2} \tag{A18}$$

where the value of $f(\infty)$ is numerically determined by Shingu et al. [30]. Expressing ℓ from (A18) we obtain Eq. (7).

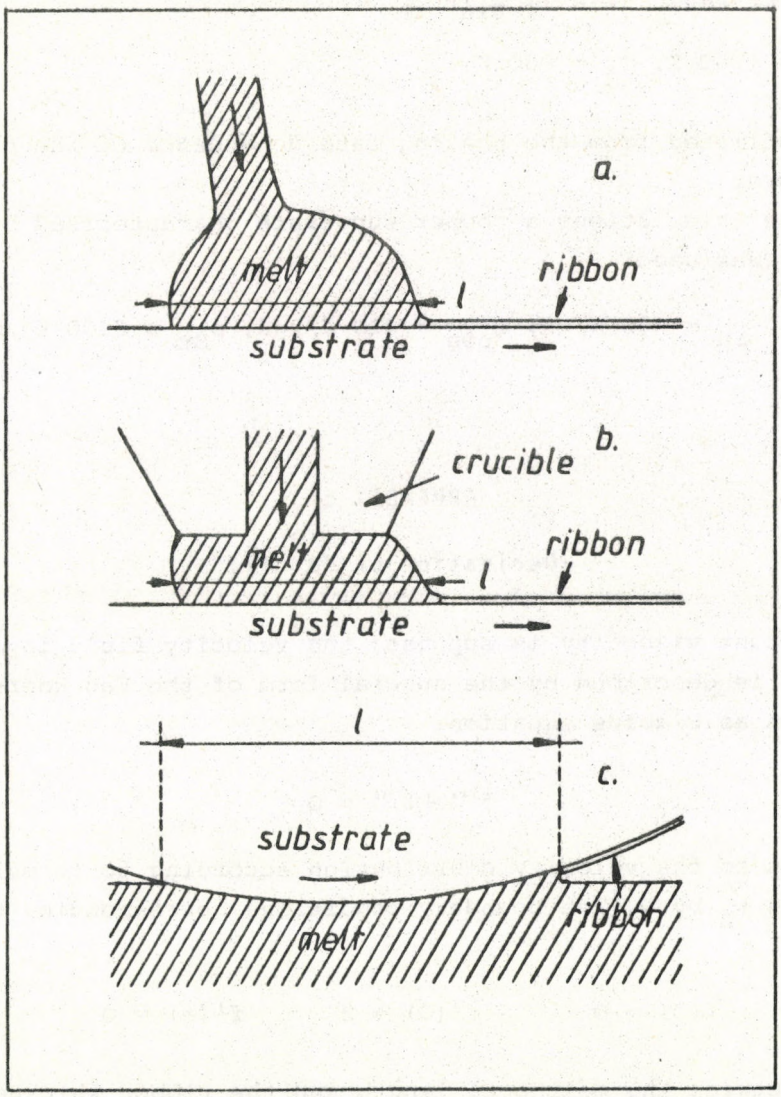

Fig. 1. Schematic drawing of the melt pool appearing in different continuous casting methods:

a) melt spinning,
b) planar flow casting,
c) melt extraction.

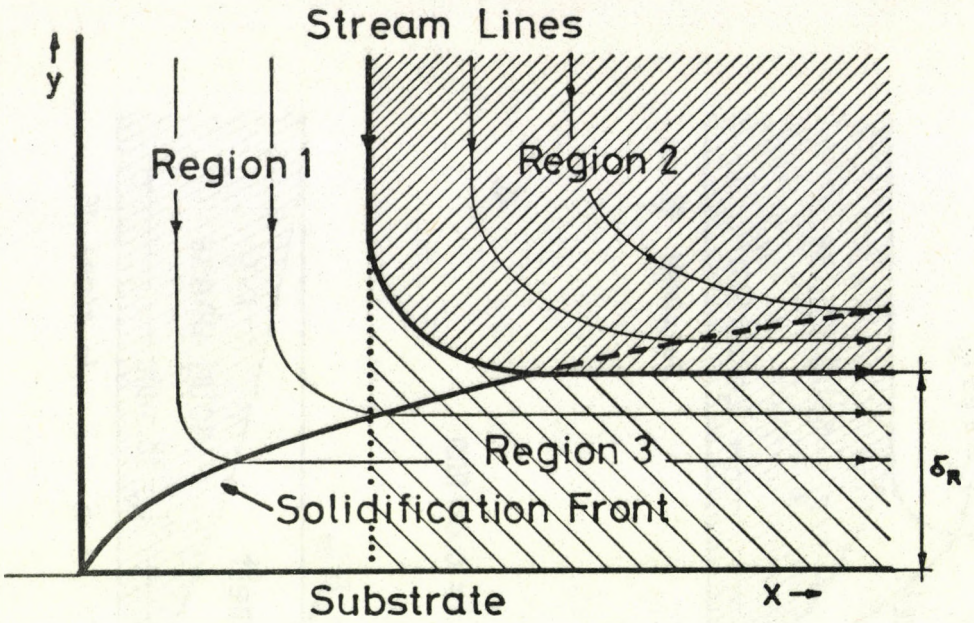

Fig. 2. Construction of the melt pool according to the method of den Decker and Drevers

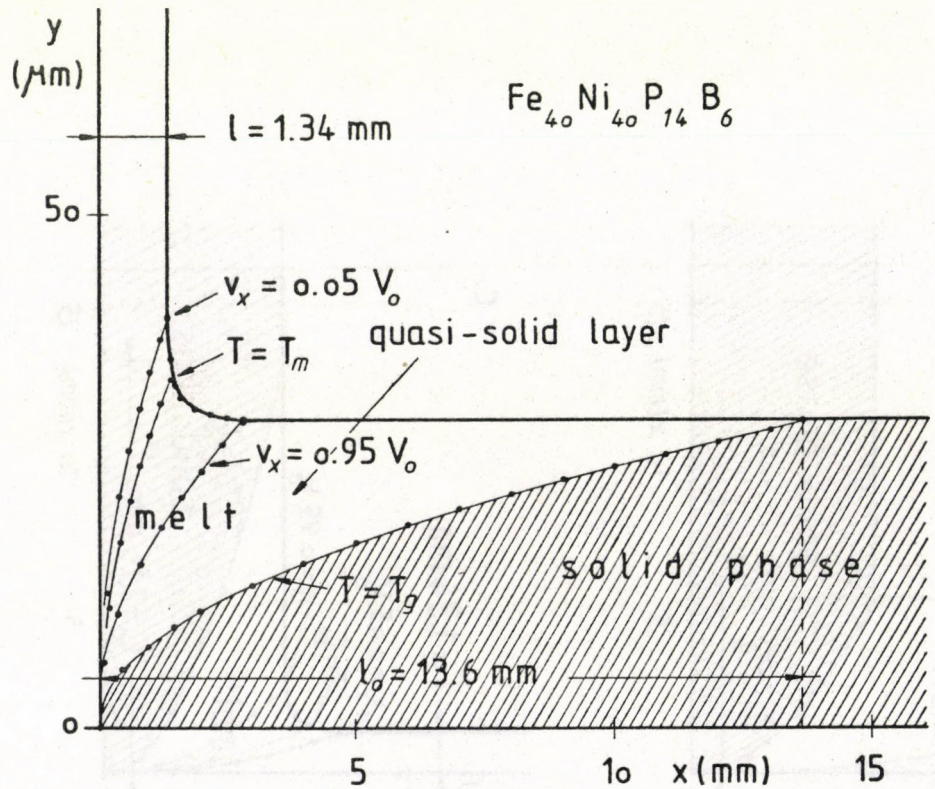

Fig. 3. The structure of the melt pool calculated for V_o = 30 m/s and δ_R = 30 µm in case of $Fe_{40}Ni_{40}P_{14}B_6$

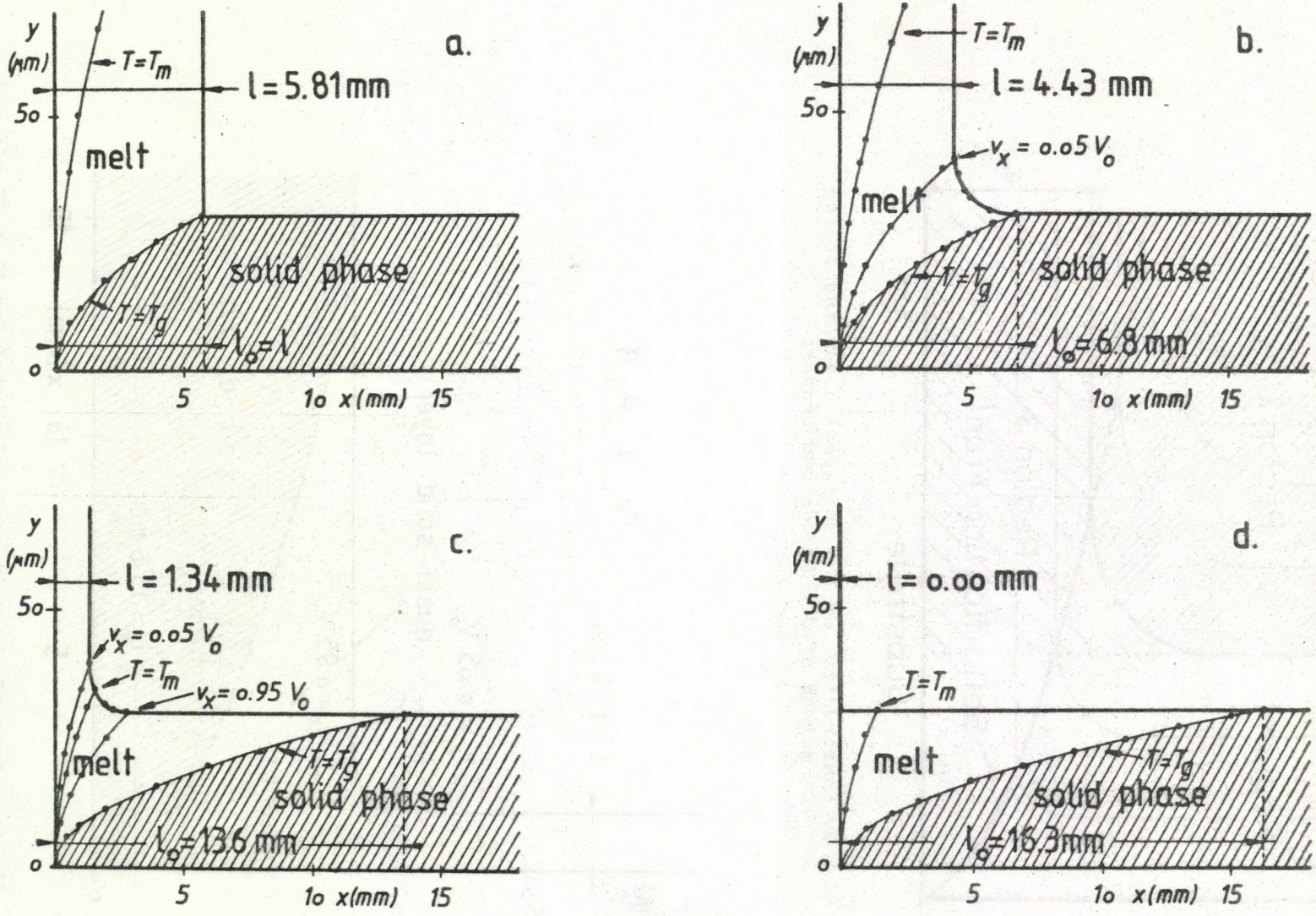

Fig. 4. Melt pool structures calculated for V_o = 30 m/s and δ_R = 30 µm using different viscosity functions: a) $\nu = 0$, b) $\nu = \nu_F(T_M)$, c) $\nu = \nu_F(T)$, d) $\nu = \infty$.

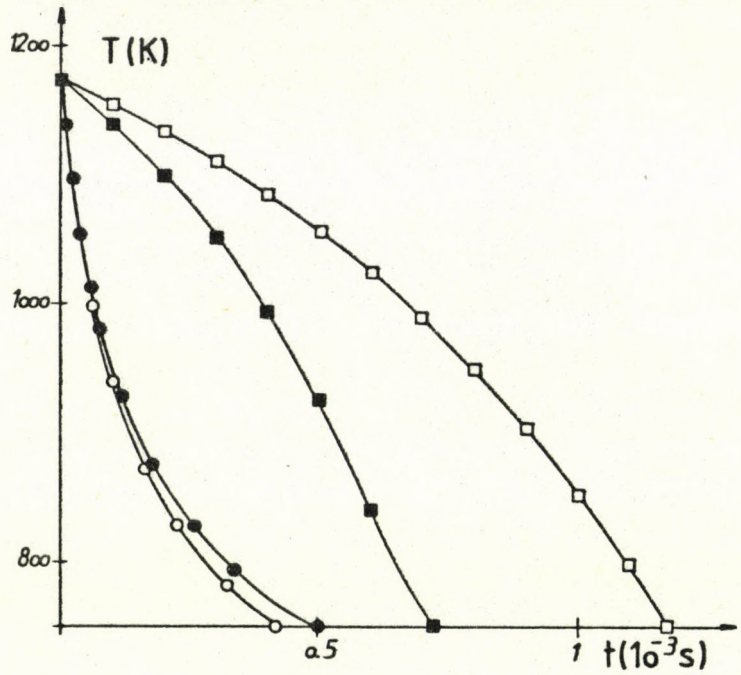

Fig. 5. Cooling curves calculated for different viscosity functions along stream lines corresponding to δ_R = 30 µm (V_o = 30 m/s).
(□: ν = o, ■: ν = $\nu_F(T_M)$, o: ν = $\nu_F(T)$, ●: ν = ∞)

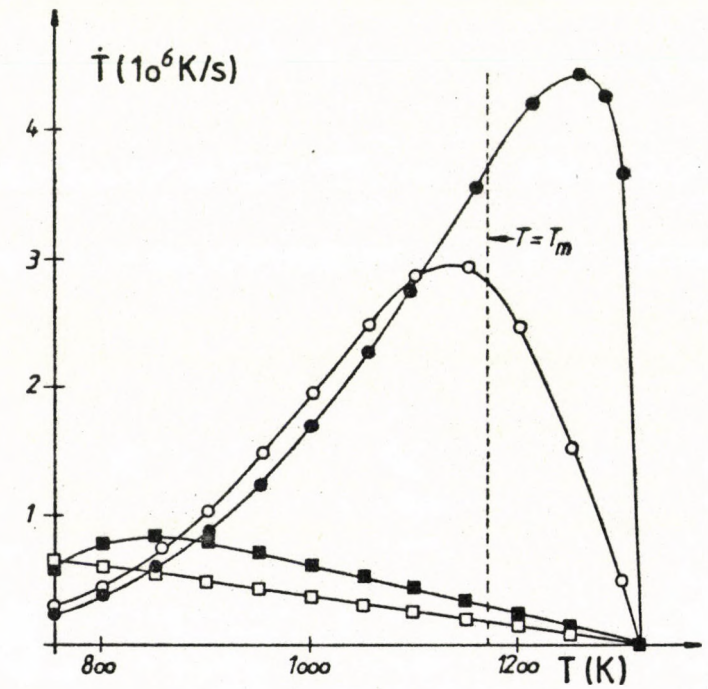

Fig. 6. Momentary quenching rate vs. actual temperature calculated along stream lines correspondig to δ_R = 30 µm.
(□: ν = o, ■: ν = $\nu_F(T_M)$, o: ν = $\nu_F(T)$, ●: ν = ∞)

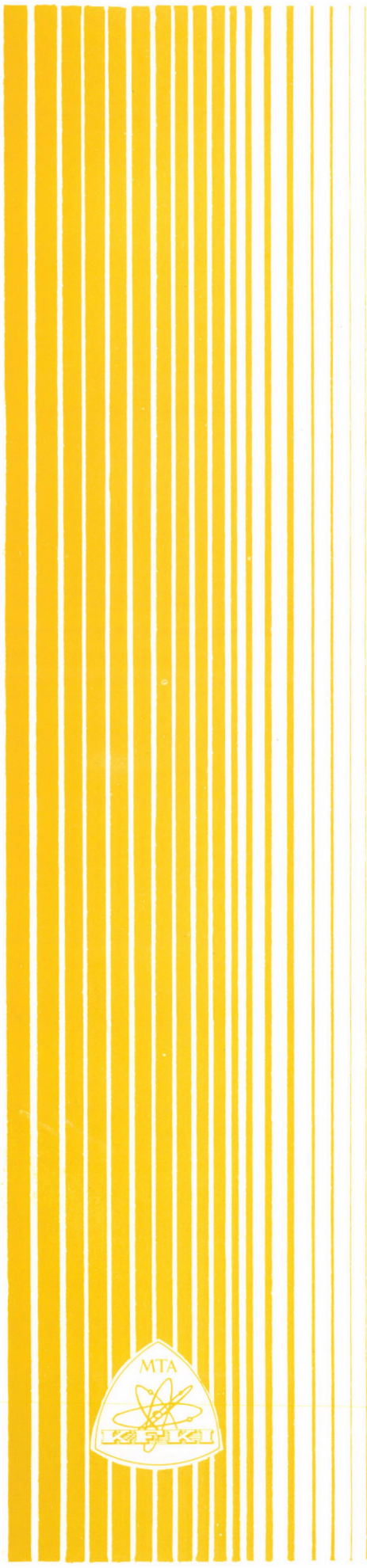

Kiadja a Központi Fizikai Kutató Intézet
Felelős kiadó: Kroó Norbert
Szakmai lektor: Lovas Antal
Nyelvi lektor: Kemény Tamás
Gépelte: Végvári Istvánné
Példányszám: 280 Törzsszám: 84-289
Készült a KFKI sokszorosító üzemében
Felelős vezető: Nagy Károly
Budapest, 1984. május hó